THE JOURNAL OF PHYSICAL CHEMISTRY C

pubs.acs.org/JPCC Article

Spreading Dynamics of Water Droplets on a Completely Wetting Surface

Selemon Bekele, Oliver G. Evans, and Mesfin Tsige*

Cite This: J. Phys. Chem. C 2020, 124, 20109–20115 Read Online

ACCESS | Metrics & More | Article Recommendations | Supporting Information

ABSTRACT: The spreading of water droplets of varying sizes on a completely wetting surface where the kinetics of spreading are controlled by hydrogen bonding between substrate and water molecules is modeled for the first time using atomistic molecular dynamics simulations. The spreading observed is characterized by the bulk part of a droplet spreading over a high density monolayer of water that forms within tens of picoseconds after the droplet is placed on the surface. The monolayer exhibits two spreading regimes, each following a power law in time with different exponents, and the late stage is faster than that predicted by Tanner's law. The bulk part of the droplet initially spreads over the monolayer with increasing radius until a characteristic time t^*. Beyond t^*, it shrinks while maintaining a constant contact angle and, interestingly, the radius is described well with a first-principles model based on hydrodynamic theory. Overall, the simulation results qualitatively agree with recent experimental data.

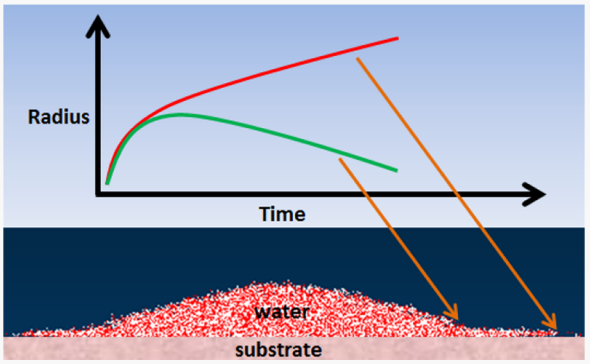

I. INTRODUCTION

When a droplet is brought in contact with a solid substrate with essentially zero speed, it may spread spontaneously under the influence of capillary and intermolecular forces.[1,2] A lot of research effort has been directed for over a century to understand the spreading dynamics of a wide variety of liquids on different types of substrates. Most of the studies focused on simple nonvolatile Newtonian droplets spreading on smooth surfaces. Theoretical investigations generally followed one of two approaches: Hydrodynamics and Molecular kinetic theory.[3]

The hydrodynamics theory[4,5] describes the characteristic features of droplet spreading in terms of an interplay between inertia, capillary, and viscous forces.[4−6] Just after a spherical drop is brought in contact with a substrate, the drop is initially set in motion because of a curvature gradient, i.e., a gradient of Laplace pressure, between the highly distorted edge of the drop close to the substrate and the spherical part sufficiently farther away.[7] In this early stage, the inertia of the drop resists the capillary driven motion, and the spreading radius has been observed to grow with time as $r(t) \sim t^{1/2}$, independent of surface wettability for liquids with low viscosity.[8,9] In the final stages, the effect of viscous forces acting in the neighborhood of the three phase contact line becomes relevant and the competition between surface tension and viscous forces results in extremely slow spreading dynamics which follows what is called Tanner's law,[10] according to which the radius of the wetted area varies with time as $r(t) \sim t^{1/10}$. The corresponding contact angle varies as $\theta(t) \sim t^{-3/10}$.[10]

In certain cases, the spreading is characterized by the emergence of a precursor film that moves ahead of the bulk part of the droplet.[11−13] In the case of a wettable surface, a precursor film consisting of one or more monomolecular layers has been observed to spread in front of the macroscopic part of the droplet with a radius varying with time as $r(t) \sim t^{1/2}$.[19]

In molecular kinetic theory,[14−18] spreading is explained in terms of the forward and backward displacement of individual molecules and/or atoms across the three phase contact line. In this case, the contact radius and contact angle vary with time as $r(t) \sim t^{1/7}$ and $\theta(t) \sim t^{-3/7}$.

The total energy dissipation has contributions from hydrodynamics flow in the bulk of the droplet, viscous dissipation in the precursor film, and adsorption and desorption of molecules to the solid substrate in the vicinity of the contact line.[19] For small contact angles, hydrodynamic dissipation is claimed to be dominant while molecular kinetic dissipation is dominant for relatively large contact angles.[20]

In contrast to classical continuum modeling efforts, the use of molecular dynamics simulations (MD) allows for studying the behavior of droplet spreading down to the molecular scale with the advantage that no assumptions on the moving contact

Received: June 7, 2020
Revised: July 27, 2020
Published: August 25, 2020

https://dx.doi.org/10.1021/acs.jpcc.0c05167
J. Phys. Chem. C 2020, 124, 20109−20115

line singularity are needed. In MD, the wetting characteristics are directly controlled by the solid−liquid interaction, which determines the equilibrium contact angle. The challenge, however, is to achieve sufficiently large drop sizes to recover a hydrodynamic regime.

Modeling the solid substrate by a smooth integrated 9−3 Lennard-Jones (LJ) potential has been observed to lead to spreading rates that were linear in time, i.e., $R \sim t$, where R is the radius of the wetted area at the solid surface.[21−23] When the solid substrates were allowed to have a molecular structure with a 12−6 LJ potential for the liquid−solid interactions, the spreading rates were found to follow the $R^2 \sim log(t)$ behavior.[24]

Sessile droplets with two-dimensional and cylindrical configurations have been considered in previous numerical studies[24−29] focusing mostly on the spreading of a precursor film. In their investigations on the spreading dynamics of liquid drop on a solid substrate, De Coninck et al.[26] observed that the spreading rate of the precursor film varies with time as $r(t) \sim t^{0.46\pm0.03}$. Using large hemispherical drops, Heine et al.[30] observed the $r(t) \sim t^{1/2}$ behavior for the precursor foot in agreement with the molecular kinetic model. In a subsequent study,[31] they examined the spreading dynamics of nanodroplets in a cylindrical geometry within the context of molecular kinetic theory and noted that the scaling laws in this geometry are modified such that $r(t) \sim t^{1/5}$.

Simulations by He and Hadjiconstantinou[29] showed that Tanner's law for spreading droplets could be recovered even if van der Waals effects and the resulting precursor film were limited to distances of the order of three atomic diameters from the substrate. They suggested that the precursor theory of de Gennes[19] could be generalized to precursors of molecular thickness in which flow is not characterized by the continuum model. Investigations by Yang et al.[24] on spreading of liquid drops on solid surfaces found log behavior for the growth of the average radii of the first and second layers, but the discrepancy with power laws is attributed to vapor condensation and small sample size.

Studies by Kandlikar et al.[28] on the spreading of a liquid water droplet in contact with a platinum surface found that the spreading area is proportional to $t^{1/3}$. Other studies based on MD simulations[21,32] reported that the spreading was much slower than that observed experimentally, and close to $r^2(t) \approx log(t)$, and the precursor film was spreading linearly in time.

Recent experimental results by Kim et al.[33] on the spreading of water and silicon oil on textured superhydrophilic surfaces show various power laws for bulk radius, precursor foot radius, and fringe film radius which is the difference between the radii of the precursor and the bulk. They found that (i) the bulk radius initially increases but then shrinks in the late stage, (ii) the precursor foot radius is proportional to $t^{1/4}$, and (iii) the fringe film radius is faster than diffusive for the entire time of spreading.

The review so far indicates that the spreading of liquid droplets on solid substrates is not yet a completely understood phenomenon. In addition to acquiring fundamental insights into spreading phenomena, a thorough understanding of the spreading behavior of droplets in contact with surfaces is important for many practical applications such as coating, corrosion protection, self-cleaning surfaces,[34,35] evaporation,[36] micro- and nanofluidics,[37−43] and biotechnology[44] that rely on the spreading behavior of water droplets on surfaces. However, none of previous simulation studies have investigated the spreading dynamics of water droplets on real surfaces. In this work, we have attempted to gain a better understanding of spreading processes using large-scale molecular dynamics simulations to examine the spontaneous spreading behavior of water nanodroplets of various initial sizes on a completely wetting surface. Simulation results are used to obtain scaling relationships for describing the temporal variation of spreading radius and the effect of droplet size on the spreading characteristics. Our simulation results show similar trends as the experimental results for bulk and precursor foot radii.[33]

II. COMPUTATIONAL DETAILS

A widely used material in catalysis is aluminum oxide, often referred to as alumina. Alumina is used as a catalyst and catalyst support, as a substrate in microelectronic devices, and in many other applications. In this work, the (0001) crystallographic face of corundum α-Al_2O_3 (space group $R\bar{3}c$)[45] was used to model an OH-terminated alumina solid substrate.[46] The CLAYFF force field[46,47] was implemented to simulate the solid substrate. CLAYFF is based on an ionic (nonbonded) description of the metal−oxygen interactions associated with hydrated phases. All atoms are represented as point charges and are allowed complete translational freedom within this force field framework. Metal−oxygen interactions are based on a simple Lennard-Jones (12−6) potential combined with electrostatics.

The SPC/E model was used to simulate water.[48] The model is known to reproduce well structural and dynamic properties of bulk water. The bonds and angles of water molecules were kept fixed by employing the SHAKE algorithm. Nonbonded interactions were modeled by means of dispersive and electrostatic forces. The electrostatic interactions were modeled by a Coulombic potential. The dispersive interactions were modeled with a 12−6 LJ potential. The LJ parameters for unlike interactions were determined by Lorentz-Berthelot mixing rules.[49] The cutoff distance for all interactions was 12 Å. Long-range corrections to electrostatic interactions were treated using the particle−particle/particle mesh (PPPM) method.[50]

The LAMMPS[51] simulation package was employed for all simulations of droplets with radii ranging from 20 to 60 Å. The dimensions of the substrate in the lateral (x-y) directions were set to approximately 41.2 nm x 41.6 nm, for a total surface area of ∼1700 nm^2. The total length of the simulation box along the z direction is ∼130 Å. The dimensions of the simulation box were chosen in such a way that there was enough vacuum above and below the combined system and the lateral dimensions were large enough to ensure that periodic images of a water droplet do not interact with each other. Periodic boundary conditions were applied in the three directions. The simulations were performed in the canonical NVT ensemble at 300 K. The Nosé−Hoover thermostat[52,53] with a relaxation time of 100 fs was used to keep the system temperature fixed at 300 K. The equations of motion were solved using the velocity-Verlet algorithm with a time step of 1.0 fs. Trajectory data were saved every 2 ps. The duration of a run was dependent on the droplet size. It took 1 ns for the 20 Å droplet to completely wet the sapphire surface, while the 50 Å droplet ran out of space within 10 ns.

https://dx.doi.org/10.1021/acs.jpcc.0c05167
J. Phys. Chem. C 2020, 124, 20109−20115

III. RESULTS AND DISCUSSION

All the droplets considered had a spherical shape just before touching the substrate. Each droplet initially starts to spread due to a pressure gradient between the edge of the drop in contact with the substrate and the spherical part which is sufficiently farther away. We have observed that the water molecules frequently form and break hydrogen bonds with the substrate OH-groups. In a previous study,[54] we showed that water molecules involved in the formation and breaking of hydrogen bonds with a substrate diffused much slower than those in a bulk environment. This would have an effect on the spreading behavior of water on a hydrophilic surface with functional groups capable of forming hydrogen bonding. The shape of the droplet changes from spherical to a spherical cap over time. Figure 1 shows snapshots of a water droplet of initial spherical geometry at times t = 0 ns (a), t = 1 ns (b), and t = 12 ns (c).

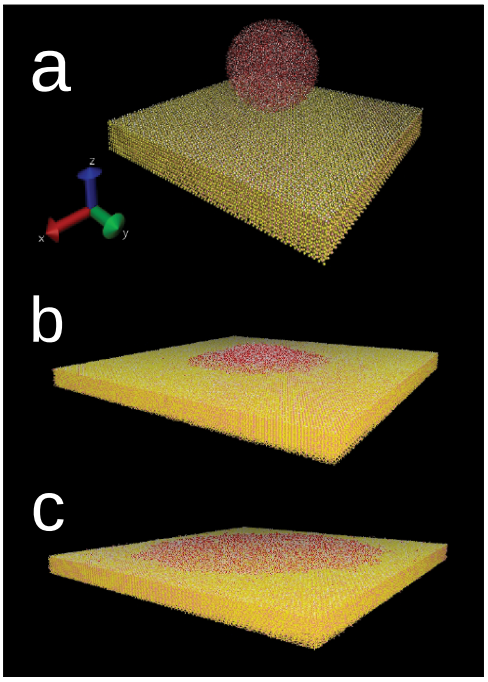

Figure 1. Snapshots of a 40 Å water droplet on sapphire at (a) t = 0 ns, (b) at t = 1 ns, and (c) t = 12 ns. Substrate surface OH groups are not shown for clarity.

Figure 2 shows the temporal evolution of the geometrical parameters associated with a droplet of initial radius R_o = 40 Å (see Figure S1 of the Supporting Information). The spreading observed is characterized by the bulk part of a droplet spreading over a high density layer of water that forms within tens of picoseconds after the droplet is placed on the surface. The high density layer of water, referred to as a monolayer in this work since it has molecular dimensions, spreads in such a way that it eventually overtakes the bulk part. Figure S2 in the supporting material shows the final water density profiles of all the droplets considered on the sapphire substrate. It is clear from the plots that complete wetting has occurred for droplets with radii $R \leq 40$ Å. For $R \geq 45$ Å, the substrate was not large enough to observe complete wetting. It appears that all droplets give rise to similar monolayer thicknesses.

The monolayer radius r_m increases monotonically with time while the height (see Figure S3 of the Supporting Information)

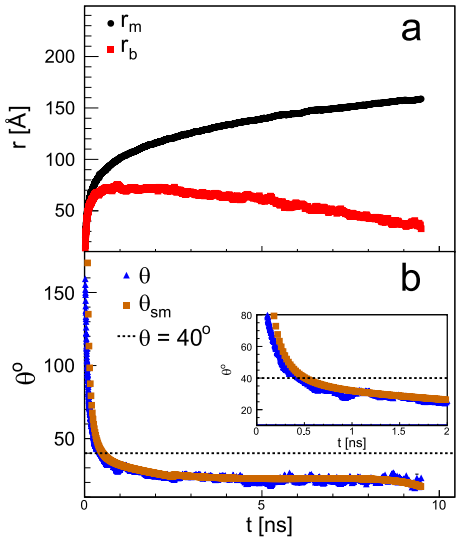

Figure 2. Time variation of the geometric parameters of a 40 Å droplet as it spreads over the sapphire substrate. (a) Monolayer radius r_m and bulk radius r_b, (b) contact angle θ and the contact angle θ_{sm} that would be obtained with the small angle approximation[55] for given values of the monolayer and bulk radii. As shown in the lower part, the small angle approximation holds for $\theta < 40°$ (dashed line). The inset highlights the early time region.

and contact angle of the bulk part decrease with time. Similar to the experimental results,[33] the bulk part spreads with increasing radius up to a point and then its radius decreases and interestingly, in the later case, maintains a constant contact angle of $\theta \approx 20^o - 25^o$. It should be noted that the bulk part retains its spherical shape throughout the spreading process but eventually disappears into the monolayer.

Mass conservation for complete wetting gives the relation $r_m^2 \propto R^3$. Figure 3 shows the square of the monolayer radius from

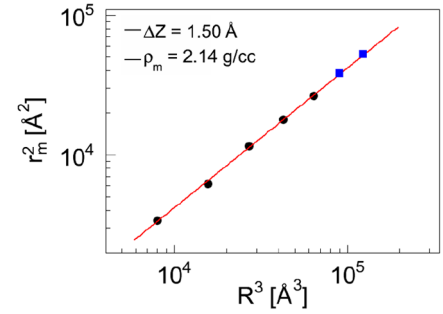

Figure 3. r_m^2 versus R^3 where R is the initial radius of a droplet. Mass conservation results in the relation $r_m^2 \propto R^3$. The line is a linear fit restricted to the region where the initial droplet radii R < = 40 Å

the simulation data plotted against the cube of the initial droplet radii. With setting the thickness of the monolayer to 1.5 Å based on the z distribution in Figure S4 of the Supporting Information, a linear fit to the data results in the monolayer density ρ_m = 2.14 g/cm^3. The fit is restricted to the region where the initial droplet radii R < = 40 Å since the larger droplets have reached the boundaries of the simulation cell, i.e., they do not have enough room for complete spreading. On the basis of the fit in Figure 3, one may estimate the maximum monolayer radius that would have been achieved for the droplets with initial radii R > 40 Å if a larger

https://dx.doi.org/10.1021/acs.jpcc.0c05167
J. Phys. Chem. C 2020, 124, 20109−20115

surface was available. For the droplets with $R > 40$ Å, we will use extrapolated values (square data points in Figure 3) for a discussion of the scaling behaviors of the monolayers.

The key result from this part of the investigation is that the monolayer spreading shows two power law regimes which may be fit to the expression

$$r_m(t) = At^n \quad (1)$$

Figure 4 shows the monolayer radius R vs time on sapphire surface for different initial radii of the droplets on logarithmic

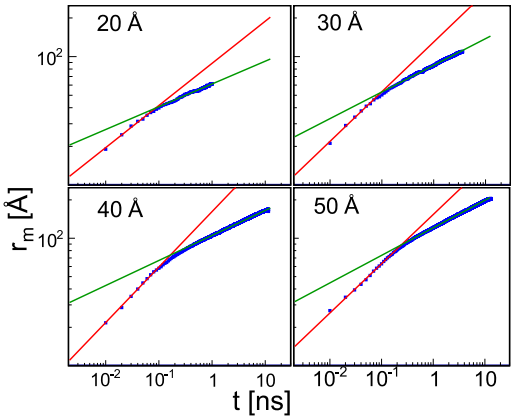

Figure 4. Monolayer radius vs time on a log–log plot. The lines indicate the regimes with different spreading behaviors. The red and green lines are power law fits to the data points corresponding, respectively, to times smaller and greater than 200 ps.

axes. For times later than 200 ps, we observe a scaling consistent with $r \sim t^{1/5}$ as the best fit to eq 1. It turns out that initial radius does have an influence on the spreading but only through the prefactor as shown in Table 1. The exponent n is

Table 1. Power Law Fit Parameters of the r_m vs Time Data for $t > 0.2$ ns

R_o	A	n
20 Å	61.2	0.18
30 Å	85.6	0.21
40 Å	105.2	0.20
50 Å	120.7	0.22

always very close to 1/5. The prefactor increases as the radius increases, such that large drops spread faster. The fit results for times earlier than 200 ps are given in Table 2. In this regime, the capillary driven motion overcomes the inertia of the droplet and forces it to adopt a spherical cap shape.[8,9] In this case, the spreading still follows a power law but the radius of the droplet affects both the prefactor and the exponent. It appears that the larger the droplet, the faster it spreads until the transition point is reached.

Table 2. Power Law Fit Parameters of the r_m vs Time Data for 0.02 < t 0.2 ns

R_o	A	n
20 Å	88.64	0.33
30 Å	129.92	0.39
40 Å	161.83	0.44
50 Å	153.54	0.39

We observe a significantly slower growth, $r_m(t) \sim t^{1/5}$, in the late stages of spreading irrespective of droplet size (see Table 1), but one that is faster than the prediction by Tanner's law ($r_m(t) \sim t^{1/10}$). These departures in behavior may be due to molecular structure of the substrate as well as the types of the interparticle interactions involved. In contrast to previous experimental and theoretical results, the monolayer radius does not suggest diffusive behavior for which $R(t) \sim t^{1/2}$, which is also the obvious theoretical expectation, on the grounds that phenomena at scales below the hydrodynamic continuum are dominated by molecular diffusion. On the basis of the fact that the droplets completely wet the surface resulting eventually in a monolayer, the results for the late stage of spreading rule out a diffusive regime at larger time scales, at least for the droplet sizes considered in this work.

We would like to compare our simulation results with recent experimental results by Kim et al.[33] on the spreading of water and silicon oil droplets of various radii on textured superhydrophilic surfaces. They found the precursor foot radius or the monolayer radius to follow $r_m \sim t^{1/4}$ which is slightly faster than the $r_m \sim t^{1/5}$ we found from our simulations. We would like to note that the monolayer radii from the simulations initially increase at a much faster rate than $t^{1/4}$ (Table 2) and then change to a slower rate of $t^{1/5}$ (Table 1) at the late stage. Our bulk radius data, shown in Figure 2 and also in Figure S3 for all the droplets, show similar behavior as the experimental bulk radii shown in Figure 8 of ref 33, i.e., the bulk radius increases initially and then shrinks in the late stage. Furthermore, they predicted the initial increase to be proportional to $t^{1/4}$ and the late decrease to be proportional to $t^{1/2}$ and a fit to their experimental data shows a good agreement with their prediction. In Figure 5, we show that

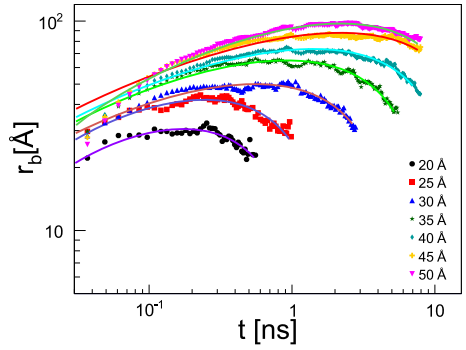

Figure 5. Time evolution of the bulk radius. The solid lines are fitting curves with the model $r_b \sim At^{1/4} - Bt^{1/2}$ provided in ref 32.

their prediction also agrees well with our simulation data especially in the late stage. We also computed the fringe film radius ($r_m - r_b$) from our simulations in order to compare with the experimental results. Interestingly, our simulation (see Figure 6) and the experiment show a similar dependence of $t^{2/3}$, which is faster than a diffusive behavior of $t^{1/2}$, for the fringe film radius. Put together, our simulation results help to illuminate some of the key experimental findings.

What is missing from the experiments is the behavior of droplet height as a function of time. Figure 7 shows droplet heights scaled by their initial droplet radius for all droplets. The data collapse onto a single curve when the time is scaled by $(A/R_0)^{10/3}$, where A is the power law coefficient and increase as $t^{3/10}$.

https://dx.doi.org/10.1021/acs.jpcc.0c05167
J. Phys. Chem. C 2020, 124, 20109−20115

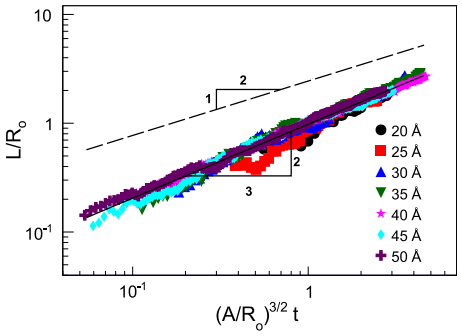

Figure 6. Time evolution of the scaled fringe film radius where $L = r_m - r_b$, A is the power law coefficient, and R_0 is the initial droplet radius.

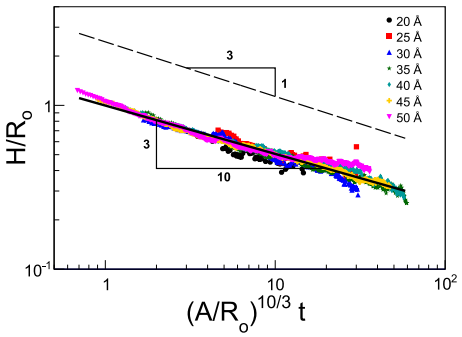

Figure 7. Time evolution of the scaled droplet height, where A is the power law coefficient and R_0 is the initial droplet radius.

IV. HYDRODYNAMICS THEORY

Much of the computational work in the literature deals with mostly viscous liquids with liquid−liquid and liquid−solid interactions modeled with simple Lennard-Jones potentials. The spreading behaviors observed with such systems exhibit spreading characteristics only without the reduction in the bulk radius in the presence of an expanding precursor film. The spreading behavior of water droplets on sapphire involves both spreading and shrinkage of the bulk part as a result of mass conservation that couples the monolayer radius to the bulk radius. Starov et al.[55] have experimentally observed behavior similar to what we see in our simulation data with silicon oil droplets on dry and fully saturated porous substrates. They have developed a hydrodynamic theory making use of the small angle approximation to describe their data. Thinking along the same lines, we argue that the motion of the bulk part of the droplet above the monolayer is a superposition of two motions: the spreading of the drop over the monolayer which leads to an expansion of the drop base, and imbibition into the monolayer causing the drop base to shrink. The spreading behavior of the bulk part of the droplet is thus a result of the interplay between the two competing processes. The time dependence of the bulk radius is thus characterized by a fast rise to a maximum and a slow decrease toward zero in the final complete wetting state.

Following the work of Starov et al.[55] with spreading of nonvolatile liquids over porous substrates, we assume that the decrease with time of the drop volume above the monolayer is determined only by the imbibition into the monolayer. This implies a dependence of the drop volume, V, only on the slow time scale. The whole spreading process can be subdivided into two stages: (1) A first stage in which the drop spreads with constant volume approximately and the imbibition into the monolayer may be neglected. (2) A second slow stage, when the spreading process is almost already over, and the evolution is determined by the imbibition into the monolayer. For times where the small angle approximation holds, the governing equations for both the droplet base radius r_b and the monolayer radius r_m are given by[55]

$$\frac{dr_b}{dt} = 0.1\left(\frac{4(V_o - \pi m\Delta r_m^2)}{\pi}\right)^{0.3}\left(\frac{10\gamma\omega}{\eta}\right)^{0.1}\frac{1}{(t+t_o)^{0.9}} - \frac{1}{3}\frac{\pi m\Delta K_p p_c r_b/\eta}{(V_o - \pi m\Delta r_m^2)\ln\left(\frac{r_m}{r_b}\right)}$$

$$\frac{dr_m}{dt} = \frac{K_p p_c/\eta}{r_m \ln\left(\frac{r_m}{r_b}\right)} \quad (2)$$

where V_o is the initial volume of the droplet, and γ and η are the surface tension and the dynamic viscosity of the liquid, respectively. Δ is the monolayer thickness, m is the porosity, ω is the lubrication coefficient, K_p is the permeability of the monolayer, and p_c is the effective capillary pressure in the monolayer; t_o is the duration of the inertial stage of spreading when the capillary regime of spreading is not applicable. Using a 4^{th} order Runge−Kutta algorithm, the data for each droplet are fit to the coupled differential expression given in eq 2. The value of t_o is set to 0.01 ns, the surface tension γ is fixed to the SPC/E value of 62.5 mN/m, and the dynamic viscosity η is left as a fit parameter except for the 50 Å droplet for which a reasonable fit could not be obtained and is set to the SPC/E value of 0.729 mPa-s. The resulting fit parameters are given in Table 3. As shown in Figure 8, the model very well describes both the monolayer and bulk data qualitatively within the range of its validity which is the regime of low contact angles. This result suggests that the theory developed for micro-droplets appears to work even at the nanoscale.

Table 3. Fit Parameters Obtained Using the Runge-Kutta Algorithm on the Coupled eqs 2[a]

R_o	η	ω	mΔ	$K_p p_c$
20 Å	0.200	9.52×10^{-2}	2.93	0.002
30 Å	0.203	1.15×10^{-3}	3.03	0.001
35 Å	0.260	7.51×10^{-4}	3.22	0.002
40 Å	0.198	5.36×10^{-4}	3.09	0.002

[a] γ and η are the surface tension and the dynamic viscosity of the liquid, respectively. ω is the lubrication coefficient, Δ is the monolayer thickness, m is the porosity, K_p is the permeability of the monolayer, and p_c is the effective capillary pressure in the monolayer.

The theory also predicts a scaling of the monolayer radius r_m at complete wetting with respect to the maximum monolayer radius r_{max} and the time t_{max} taken by the monolayer to attain its maximum radius. The bulk radius r_b with respect to the maximum value $r_{b_{max}}$ it attains when the monolayer transitions from the earliest power law regime to the late power law regime also shows a scaling behavior. Figure 9 shows the raw and scaled data for the monolayer and the bulk radii for all droplets. Each monolayer radius is scaled by the corresponding maximum radius achieved at complete wetting for initial radius $R_0 <= 40$ Å. Spreading time is scaled by the maximum time required for complete wetting. As mentioned before, the

https://dx.doi.org/10.1021/acs.jpcc.0c05167
J. Phys. Chem. C 2020, 124, 20109−20115

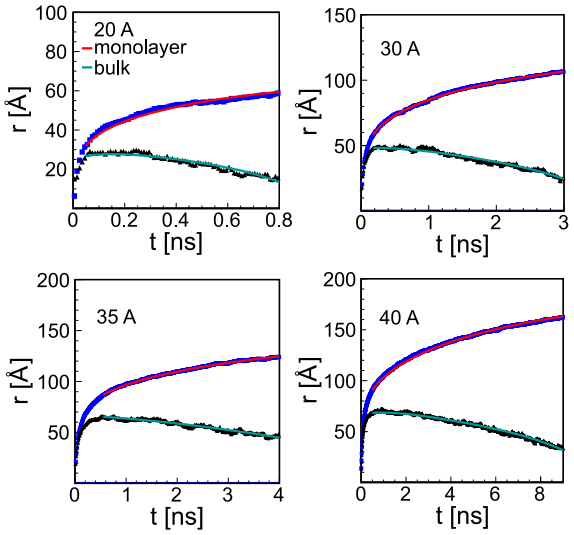

Figure 8. R vs time fits using a fourth order Runge−Kutta algorithm with the coupled differential expression given in eq 2.

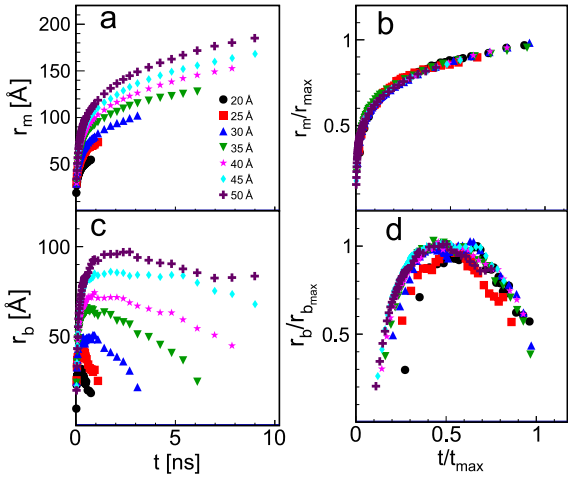

Figure 9. (a)Monolayer radius r_m versus time, (b) scaled monolayer radius r_m/r_{max} vs t/t_{max} where r_{max} is the maximum radius of a monolayer at complete wetting and t_{max} is the time to attain r_{max}, (c) bulk radius r_b versus time, and (d) scaled bulk radius $r_b/r_{b_{max}}$ vs t/t_{max} where $r_{b_{max}}$ is the maximum bulk radius attained.

maximum monolayer radii for the droplets with initial radii 45 and 50 Å are obtained by extrapolation using the fit shown in Figure 3, and the corresponding maximum times for these two cases are estimated using eq 1 for the late stage of spreading. As shown in Figure 9b,d, the data appear to collapse onto single master curves when r_m/r_{max} and $r_b/r_{b_{max}}$ are plotted as a function of t/t_{max}.

V. SUMMARY

Water in contact with surfaces is ubiquitous, and the challenge of understanding and quantifying this interaction has immense implications for the design of materials in many different applications including medicine, sustainability, and engineering applications. To this end, the spreading behavior of water droplets of varying sizes on a completely wetting surface has been investigated using fully atomistic molecular dynamic simulations. The dynamics observed are characterized by a monolayer of high density water of molecular dimensions that moves ahead of the main bulk part of the droplet. The bulk part of the droplet initially spreads over the monolayer with increasing radius until a characteristic time $t^* \sim 0.1-0.5$ ns where the monolayer changes from one power law behavior to another. For times after t^*, it shrinks while maintaining a constant contact angle until it disappears altogether and only a monolayer of water remains on the substrate. The monolayer motion exhibits two spreading regimes, each following a power law in time with different exponents. The values of the exponents indicate a nondiffusive motion of the monolayer edge in both time regimes. The late stage monolayer dynamics are faster than that predicted by Tanner's law. Whether this is typical of completely wetting surfaces or is somehow related to the liquid being water remains to be resolved. A first-principles model based on hydrodynamic theory has been shown to describe the spreading data rather well in the regime where the low contact angle approximation holds. The scaling of both the monolayer and the bulk radii by the maximum monolayer radius r_{max} and time by the maximum time t_{max} for the monolayer to reach r_{max} collapses the data onto single master curves.

■ ASSOCIATED CONTENT

Supporting Information

The Supporting Information is available free of charge at https://pubs.acs.org/doi/10.1021/acs.jpcc.0c05167.

Cartoon representation of the water droplet, water droplet profiles, small angle approximation, number distributions of water molecules in monolayer, mass conservation, time dependence of monolayer and base radii (PDF)

■ AUTHOR INFORMATION

Corresponding Author

Mesfin Tsige − *Department of Polymer Science, The University of Akron, Akron, Ohio 44325, United States;* orcid.org/0000-0002-7540-2050; Email: mtsige@uakron.edu

Authors

Selemon Bekele − *Department of Polymer Science, The University of Akron, Akron, Ohio 44325, United States*

Oliver G. Evans − *Department of Polymer Science, The University of Akron, Akron, Ohio 44325, United States*

Complete contact information is available at: https://pubs.acs.org/10.1021/acs.jpcc.0c05167

Notes

The authors declare no competing financial interest.

■ ACKNOWLEDGMENTS

This work was supported by the National Science Foundation (DMR-1912329). The authors would like to thank A. Dhinojwala and Gary Grest for helpful discussions.

■ REFERENCES

(1) Semal, S.; Voue, M.; de Ruijter, M. J.; Dehuit, J.; De Coninck, J. Dynamics of spontaneous spreading on heterogeneous surfaces in a partial wetting regime. *J. Phys. Chem. B* **1999**, *103*, 4854−61.

(2) Glasner, K. B. Spreading of droplets under the influence of intermolecular forces. *Phys. Fluids* **2003**, *15*, 1837−1842.

(3) Chen, L.; Bonaccurso, E. Effects of surface wettability and liquid viscosity on the dynamic wetting of individual drops. *Phys. Rev. E* **2014**, *90*, 022401.

(4) Shikhmurzaev, Y. D. Moving contact lines in liquid/liquid/solid systems. *J. Fluid Mech.* **1997**, *334*, 211−249.
(5) Cox, R. G. The dynamics of the spreading of liquids on a solid surface. *J. Fluid Mech.* **1986**, *168*, 169−194.
(6) Voinov, O. V. Hydrodynamics of wetting. *Fluid Dyn.* **1977**, *11*, 714−721.
(7) Eddi, A.; Winkels, K. G.; Snoeijer, J. H. Short time dynamics of viscous drop spreading. *Phys. Fluids* **2013**, *25*, 013102−10.
(8) Biance, A.-L.; Clanet, C.; Quéré, D. First steps in the spreading of a liquid droplet. *Phys. Rev. E* **2004**, *69*, 016301−4.
(9) Bird, J. C.; Mandre, S.; Stone, H. A. Short-Time dynamics of partial wetting. *Phys. Rev. Lett.* **2008**, *100*, 234501−4.
(10) Tanner, L. The spreading of silicone oil drops on horizontal surfaces. *J. Phys. D: Appl. Phys.* **1979**, *12*, 1473−1484.
(11) Decamps, C.; De Coninck, J. Dynamics of spontaneous spreading under electrowetting conditions. *Langmuir* **2000**, *16*, 10150−3.
(12) Webb, E. B., III; Grest, G. S.; Heine, D. R. Precursor Film Controlled Wetting of Pb on Cu. *Phys. Rev. Lett.* **2003**, *91*, 236102−4.
(13) Pierce, F.; Perahia, D.; Grest, G. S. Spreading of Liquid Polymer Droplets on Permeable Polymeric Surfaces. *EPL* **2009**, *86*, 64004−p5.
(14) Blake, T. D.; Haynes, J. M. Kinetics of liquid/liquid displacements. *J. Colloid Interface Sci.* **1969**, *30*, 421−43l.
(15) Cherry, B. W.; Holmes, C. M. Kinetics of wetting of surfaces by polymers. *J. Colloid Interface Sci.* **1969**, *29*, 174−6.
(16) Blake, T. D. PhD Thesis University of Bristol, 1968.
(17) Blake, T. D.; berg, J.C. *Dynamic Contact angles and wetting kinetics*, in: J., C Berg (Ed.) Wettebility Marcel Dekker, New York, 1993, 251−309.
(18) Ruckenstein, E.; Dunn, C. S. Slip Velocity during Wetting of Solids. *J. Colloid Interface Sci.* **1977**, *59*, 135−138.
(19) de Gennes, P. G. Wetting: Statics and Dynamics. *Rev. Mod. Phys.* **1985**, *57*, 827−863.
(20) Brochard-Wyart, F.; de Gennes, P. G. Dynamics of partial wetting. *Adv. Colloid Interface Sci.* **1992**, *39*, 1−11.
(21) Nieminen, J.; Abraham, D.; Karttienen, M.; Kaski, K. Molecular dynamics of a microscopic droplet on solid surface. *Phys. Rev. Lett.* **1992**, *69*, 124−127.
(22) Nieminen, J. A.; Ala-Nissila, T. Spreading dynamics of polymer microdroplets: a molecular-dynamics study. *Phys. Rev. E: Stat. Phys., Plasmas, Fluids, Relat. Interdiscip. Top.* **1994**, *49*, 4228−4236.
(23) van Remoortere, P.; Mertz, J. E.; Scriven, L. E.; Davis, H. T. Wetting behavior of a Lennard-Jones system. *J. Chem. Phys.* **1999**, *110*, 2621−2628.
(24) Yang, J. X.; Koplik, J.; Banavar, J. R. Molecular dynamics of drop spreading on solid surfaces. *Phys. Rev. Lett.* **1991**, *67*, 3539−42.
(25) Heslot, F.; Fraysse, N.; Cazabat, A. M. Molecular layering in the spreading of wetting liquid drops. *Nature* **1989**, *338*, 640−642.
(26) De Coninck, J.; Ortona, U. D.; Koplik, J.; Banavar, J. Terraced spreading of chain molecules via molecular dynamics. *Phys. Rev. Lett.* **1995**, *74*, 928−931.
(27) de Ruijter, M.; Blake, T. D.; Clarke, A.; De Coninck, J. Droplet spreading: a tool to characterize surfaces at the microscopic scale. *J. Pet. Sci. Eng.* **1999**, *24*, 189−198.
(28) Kandlikar, S. G.; Maruyama, S.; Steinke, M. E.; Kimura, T. Molecular dynamics simulation and measurement of contact angle of water droplet on a platinum surface *ASME Proc. Int. Mechanical Engineering Congress and Exposition* (11−16 November **2001**) paper IMECE 01−2832.
(29) He, G.; Hadjiconstantinou, N. G. A molecular view of Tanner's law: molecular dynamics simulations of droplet spreading. *J. Fluid Mech.* **2003**, *497*, 123−132.
(30) Heine, D. R.; Grest, G. S.; Webb, E. B., III Spreading dynamics of polymer nanodroplets. *Phys. Rev. E: Stat. Phys., Plasmas, Fluids, Relat. Interdiscip. Top.* **2003**, *68*, 061603−10.
(31) Heine, D. R.; Grest, G. S.; Webb, E. B., III Spreading dynamics of polymer nanodroplets in cylindrical geometries. *Phys. Rev. E* **2004**, *70*, 011606−10.
(32) Yang, J. X.; Koplik, J.; Banavar, J. R. Terraced spreading of simple liquids on solid surfaces. *Phys. Rev. A: At., Mol., Opt. Phys.* **1992**, *46*, 7738−7749.
(33) Kim, S. J.; Kim, J.; Moon, M.-W.; Lee, K.-R.; Kim, H.-Y. Experimental study of drop spreading on textured superhydrophilic surfaces. *Phys. Fluids* **2013**, *25*, 092110.
(34) Blossey, R. Self-cleaning surfaces - virtual realities. *Nat. Mater.* **2003**, *2* (5), 301−306.
(35) Lafuma, A.; Quéré, D. Superhydrophobic states. *Nat. Mater.* **2003**, *2* (7), 457−460.
(36) Li, Q.; Wang, B.; Chen, Y.; Zhao, Z. Wetting and evaporation of argon nanodroplets on smooth and rough substrates: Molecular dynamics simulations. *Chem. Phys. Lett.* **2016**, *662*, 73−79.
(37) Carrilho, E.; Martinez, A. W.; Whitesides, G. M. Understanding Wax Printing: A Simple Micropatterning Process for Paper-Based Microfluidics. *Anal. Chem.* **2009**, *81* (16), 7091−7095.
(38) Wang, S.; Wang, T.; Ge, P.; Xue, P.; Ye, S.; Chen, H.; Li, Z.; Zhang, J.; Yang, B. Controlling Flow Behavior of Water in Microfluidics with a Chemically Patterned Anisotropic Wetting Surface. *Langmuir* **2015**, *31* (13), 4032−4039.
(39) Xia, D.; Johnson, L. M.; López, G. P. Anisotropic Wetting Surfaces with One2010Dimesional and Directional Structures: Fabrication Approaches, Wetting Properties and Potential Applications. *Adv. Mater.* **2012**, *24* (10), 1287−1302.
(40) Schutzius, T. M.; Graeber, G.; Elsharkawy, M.; Oreluk, J.; Megaridis, C. M. Morphing and vectoring impacting droplets by means of wettability-engineered surfaces. *Sci. Rep.* **2015**, *4*, 7029−1−7.
(41) Bliznyuk, O.; Jansen, H. P.; Kooij, E. S.; Zandvliet, H. J.; Poelsema, B. Smart Design of Stripe-Patterned Gradient Surfaces to Control Droplet Motion. *Langmuir* **2011**, *27* (17), 11238−11245.
(42) Prakash, S.; Piruska, A.; Gatimu, E. N.; Bohn, P. W.; Sweedler, J. V.; Shannon, M. A. Nanofluidics: systems and applications. *IEEE Sens. J.* **2008**, *8*, 441−450.
(43) Bocquet, L.; Charlaix, E. Nanofluidics, from bulk to interfaces. *Chem. Soc. Rev.* **2010**, *39*, 1073−1095.
(44) Zhang, Y.; Ozdemir, P. Microfluidic DNA amplification - a review. *Anal. Chim. Acta* **2009**, *638*, 115−125.
(45) Tobbens, D. M.; Stusser, N.; Knorr, K.; Mayer, H. M.; Lampert, G. E9: The new high-resolution neutron powder diffractometer at the Berlin neutron scattering center. *Mater. Sci. Forum* **2001**, *378*, 288−293.
(46) Cygan, R. T.; Liang, J.; Kalinichev, A. G. Molecular Models of Hydroxide, Oxyhydroxide, and Clay Phases and the Development of a General Force Field. *J. Phys. Chem. B* **2004**, *108* (4), 1255−1266.
(47) Argyris, D.; Ho, T.; Cole, D. R.; Striolo, A. Molecular Dynamics Studies of Interfacial Water at the Alumina Surface. *J. Phys. Chem. C* **2011**, *115*, 2038−2046.
(48) Berendsen, H. J. C.; Grigera, J. R.; Straatsma, T. P. The missing term in effective pair potentials. *J. Phys. Chem.* **1987**, *91* (24), 6269−6271.
(49) Allen, M. P.; Tildesley, D. J. *Computer Simulation of Liquids*. Oxford University Press: Oxford, U.K. 2004.
(50) Essmann, U.; Perera, L.; Berkowitz, M. L.; Darden, T.; Lee, H.; Pedersen, L. G. A smooth particle mesh Ewald method. *J. Chem. Phys.* **1995**, *103* (19), 8577−8593.
(51) Plimpton, S. Fast Parallel Algorithms for Short-Range Molecular Dynamics. *J. Comput. Phys.* **1995**, *117*, 1−19.
(52) Nose, S. Molecular-Dynamics, A Method for Simulations in the Canonical Ensemble. *Mol. Phys.* **1984**, *52* (2), 255−268.
(53) Hoover, W. G. Canonical Dynamics Equilibrium Phase-Space Distributions. *Phys. Rev. A: At., Mol., Opt. Phys.* **1985**, *31* (3), 1695−1697.
(54) Bekele, S.; Tsige, M. Characterizing the Hydrophobicity of Surfaces Using the Dynamics of Interfacial Water Molecules. *J. Phys. Chem. C* **2018**, *122*, 9015−9020.
(55) Starov, V. M.; Velarde, M. G.; Radke, C. Wetting and Spreading Dynamics Taylor & Frances. *Surface Science series* **2007**, *138*, 16178 DOI: 10.1201/9781420016178.